Protein Dynamics

Deutsche Ausgabe: DOI: 10.1002/ange.201603254
Internationale Ausgabe: DOI: 10.1002/anie.201603254

The Role of Dynamics and Allostery in the Inhibition of the eIF4E/eIF4G Translation Initiation Factor Complex

Nicola Salvi, Evangelos Papadopoulos, Martin Blackledge, and Gerhard Wagner**

Abstract: *Lack of regulation of the interaction between the eIF4E/eIF4G subunits of the translation initiation factor complex eIF4F is a hallmark of cancer. The inhibitor 4EGI-1 binds to eIF4E, thereby preventing association with eIF4G through an allosteric mechanism. NMR spectroscopy and MD simulations were used to obtain a mechanistic description of the role of correlated dynamics in this allosteric regulation. We show that binding of 4EGI-1 perturbs native correlated motions and increases correlated fluctuations in part of the eIF4G binding site.*

Eukaryotic translation initiation factor 4F (eIF4F), which is a complex of the cap-binding subunit eIF4E, the scaffolding protein eIF4G, and the RNA helicase eIF4A, is required for cap-dependent translation.[1] eIF4E is the least abundant component and therefore the eIF4E/eIF4G interaction determines the level of eIF4F.[2]

The eIF4E-binding proteins (4E-BPs) regulate the eIF4E/eIF4G interaction by binding to the same site as eIF4G through the same consensus motif.[3] 4E-BPs act as tumor suppressors,[4,5] whereas loss of 4E-BP expression[5,6] and 4E-BP hyperphosphorylation[7–12] are correlated with tumorigenesis and cancer growth. A promising strategy for cancer treatment is thus to develop molecules that mimic 4E-BP activity. Our group has identified an inhibitor, eIF4E/eIF4G interaction inhibitor 1 (4EGI-1), which is a promising drug candidate because it not only displaces eIF4G but also enhances the 4E-BP1/eIF4E association.[13,14] 4EGI-1 inhibits cap-dependent translation and exhibits activity against cancer cell lines and in mouse xenografts.[15,16]

4EGI-1 binds to a pocket distal to the eIF4G-binding site, between β_2 and α_1.[17] The crystal structure suggests two conformations of the binding site. With 0.6 occupancy, binding triggers a structural rearrangement in the H_{78}–L_{85} region, unfolding a 3_{10}-helix and forming an additional turn (H_{78}–S_{82}) in α_1, a conformation not seen previously in any eIF4E structure. However, with 0.4 occupancy, the inhibitor does not cause this structural rearrangement.[17] These findings indicate that 4EGI-1 acts on eIF4E through allosteric regulation by stabilizing conformers that disfavor eIF4G binding. Recently, we showed that 4E-BP1 binds to the eIF4E conformation with the short α-helix$_1$ but allows 4EGI-1 binding as well,[14] thereby supporting an inhibitor-induced population shift.

While the mechanism of the allosteric process is unclear, a predominant role of dynamics is suggested by the fact that 4EGI-1 binds to two different conformations and the eIF4G binding site is structurally unperturbed by inhibitor binding.[17]

In the present work, we used NMR relaxation data (^{15}N R_1 and R_2 rates and heteronuclear NOE ratios at 900 MHz are shown in Figure S4 of the Supporting Information, and CSA/DD cross-correlated transverse cross-relaxation rates at 750 MHz in Figure 1) in combination with Molecular Dynamics (MD) simulations to describe the population shift that occurs upon binding and to understand how changes in dynamics drive the allosteric modulation of the eIF4E/eIF4G interaction.

A single set of resonances for all assigned backbone amide peaks in eIF4E is observed.[17] Thus, there is no evidence for slow conformational exchange. There is also no indication for exchange on a μs–ms timescale because the characteristic line broadening resulting from conformational dynamics occurring at this timescale (Figure S1 in the Supporting Information) is not detected.

In order to investigate the population equilibrium present in solution, we performed a series of MD simulations. Simulation **1** comprised three 100 ns trajectories at 5 °C.

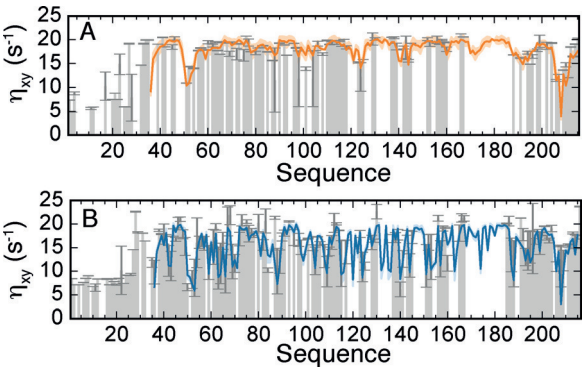

Figure 1. CSA/DD cross-correlated cross-relaxation transverse rates (η_{xy}). Experimental values (grey bars) for the GB1-eIF4E construct before (panel A) and after (panel B) the addition of 4EGI-1 (200 μM, corresponding to twice the protein concentration) are reproduced by linear combinations of the values derived from simulations **1** and **2** as described in the text. The Pearson correlation coefficient and *p* value are 0.80 and 3.44×10^{-21}, and 0.89 and 9.02×10^{-40} for panels A and B, respectively. Only data on the eI4E chain are shown.

[*] Dr. N. Salvi, Dr. E. Papadopoulos, Prof. G. Wagner
Department of Biological Chemistry and Molecular Pharmacology
Harvard Medical School, Boston (USA)
E-mail: gerhard_wagner@hms.harvard.edu
Dr. N. Salvi, Dr. M. Blackledge
Univ. Grenoble Alpes, CNRS, CEA, Institut de Biologie Structurale
Grenoble (France)
E-mail: nicola.salvi@ibs.fr

Supporting information for this article can be found under: http://dx.doi.org/10.1002/anie.201603254.

Trajectory A is calculated starting from the eIF4E chain not bound to 4EGI-1 in the crystal structure (chain B in PDB ID: 4TPW; "free-like" conformation). Trajectories B and C are started from conformations of eIF4E extracted from trajectory A after 50 and 100 ns, with randomly distributed atomic velocities. Similarly, simulation **2** contains three 100 ns trajectories started from the eIF4E chain bound to 4EGI-1 in the crystal structure (chain A in PDB ID: 4TPW; "bound-like" conformation) and from frames extracted from the former trajectory after 50 and 100 ns. Finally, simulations **1_25C** and **2_25C** comprise one 100 ns trajectory each, calculated at 25 °C and started from the two chains in the crystal structure (PDB ID: 4TPW; see Experimental Procedures in the Supporting Information).

Owing to the lack of optimized force fields for the N_7-methylated nucleotide and for 4EGI-1, ligands were removed from the PDB structure and simulations were performed with the peptide chains only. As shown in Figure S3, in analyzing our trajectories, we excluded all residues above 180 to eliminate possible errors induced by this simplification of the system (the values corresponding to those residues are nevertheless shown for the sake of completeness).

We do not observe any transition between free-like and bound-like conformations in any of our simulations, thus suggesting that this interconversion occurs on timescales longer than the rotational correlation time τ_c. Therefore, any observed NMR relaxation rate is given by $R_{obs} = x_{free}R_{free} + (1-x_{free})R_{bound}$, in which R_{obs} is the measured relaxation rate (R_1, R_2, nOe or η_{xy}), R_{free} and R_{bound} the corresponding relaxation rates of the two conformers, and x_{free} the molar fraction of the free-like conformation. Assuming that good approximations to R_{free} and R_{bound} are calculated from simulation **1** and **2**, respectively, a fit to experimental data can be used to estimate x_{free} and τ_c.

By using this fit procedure, we obtained $x_{free} = 0.90 \pm 0.07$ and $\tau_c = (17.6 \pm 0.5)$ ns. The latter value is in agreement with the result of the TRACT procedure.[17] In order to validate our results, we applied the same procedure to ^{13}C chemical shifts: $SCS_{obs} = x_{free}SCS_{free} + (1-x_{free})SCS_{bound}$, in which SCS_{obs} is the measured secondary chemical shift for $^{13}C\alpha$, $^{13}C\beta$ or $^{13}C'$ spins, and SCS_{free} and SCS_{bound} the corresponding quantities for the free- and bound-like conformers. If approximations to SCS_{free} and SCS_{bound} are calculated from simulations **1_25C** and **2_25C**, we find $x_{free} = 0.88 \pm 0.02$, which is in agreement with the relaxation-based calculation (Figure S5). Experimental data and MD trajectories used in the validation step were not used in the first fit. Importantly, the values of x_{free} determined at 5 °C and 25 °C are not significantly different, thus suggesting that the equilibrium between conformations is essentially temperature-independent over our range of temperatures.

The stability of the protein sample is very limited when 4EGI-1 is added. In this case, we were able to measure only CSA/DD cross-correlated transverse cross-relaxation rates at 750 MHz (Figure 1 B) within the sample lifetime (< 24 hours).

Comparison of the experimental data in Figure 1 shows that 4EGI-1 increases the flexibility of eIF4E throughout its sequence, and particularly in regions adjacent to the 4EGI-1 binding site: the loop between β1 and β2, part of helix α1, and the loop between the extended α1 and β3. By using the same fit procedure as above, we obtained $\tau_c = (17.0 \pm 0.2)$ ns, which is in agreement with the value determined from the first set of relaxation data, and $x_{free} = 0.42 \pm 0.02$. Our attempts to measure accurate secondary ^{13}C chemical shifts in the presence of 4EGI-1 were not successful because of the presence of the DMSO used to dissolve the compound (Figure S14). The calculated value of x_{free} thus has to be considered as a rough estimate. Interestingly, this value is remarkably close to the occupancy in the crystal structure.[14,17]

In summary, 4EGI-1 stabilizes the bound-like conformation, increasing its population to around 60 %. Our model and the absence of R_{ex} contributions suggest that 4EGI-1 affects mostly sub-τ_c dynamics. We can thus describe its allosteric effects by characterizing the difference in dynamics between simulations **1** and **2**.

We assessed the extent of correlated fluctuations by examining the magnitude of the pairwise cross-correlation coefficients c_{ij} of the Cα atoms. The value of c_{ij} can vary from 1 (completely correlated) to −1 (completely anticorrelated) motions.[18,19]

In simulation **1**, fluctuations in the β-sheet are strongly correlated from β1 to β6 (C1–C7 in Figure 2 A and Figure S6; β7 is in the part of the protein that is excluded from the analysis), which is in line with recent work suggesting that correlation is a fundamental property of β-sheets.[20] An additional correlation (C8) is found between β5 and the C-terminal part of α2, next to the eIF4G binding site. The loop bearing W_{102}, which binds to the cap, is anticorrelated to several β-strands (A2, A3 and A4), to the N-terminal part of α1 (A5) and, importantly, to the binding site of eIF4G, both directly (A1) and via the β-sheet (C8 + A2).

Our results are in agreement with the allosteric pathway connecting W_{102} to the eIF4G binding site described by Siddiqui et al.[21]

Correlations in the β-sheet (C1–C7) are still found in simulation **2** (Figures 2 B and S6). However, the C terminus of α2 is now correlated with α3 (C9), and larger correlations are also detected within the extended α1 (C10). While the W_{102} loop is anticorrelated only with the 3/10 helix around 145 (A6), anticorrelations are found between the N terminus and β2 (A11) and α1 (A10). Strong anticorrelations involve elements participating in the structural rearrangements in response to 4EGI-1: α1 and the 3/10 helix around 120 (A7); the loop between β1 and β2 and β5 (A8), and α1 (A9). One would expect these couplings to be even stronger if 4EGI-1 was included in the simulation.

In summary, the native network of correlations is fundamentally altered in the bound-like conformation. Couplings of the eIF4G binding site with the cap-binding site are dissolved, whereas new correlations involving α1 (but not α2) emerge. We explored the effect of these correlated motions in a principal component analysis (PCA) of the fluctuations of the cartesian coordinates of Cα atoms. Four and six eigenmodes were retained for simulations **1** and **2** respectively, on the basis of the scree plot in Figure S7.

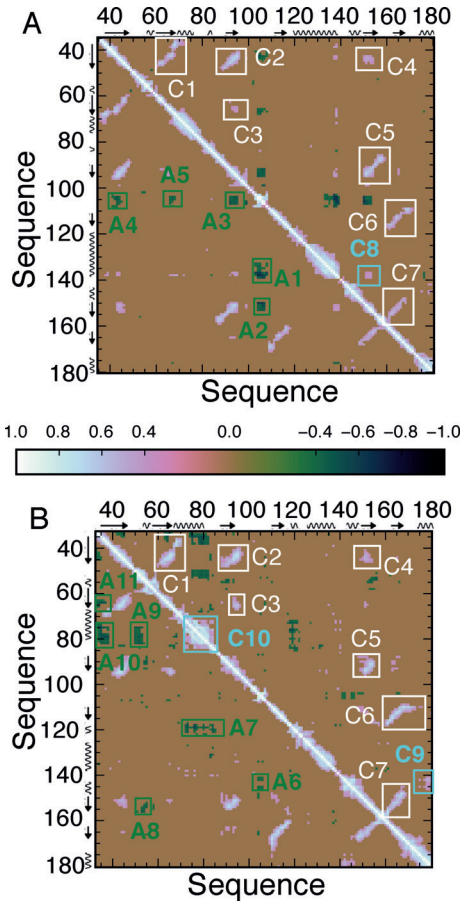

Figure 2. Dynamic cross-correlation matrix (DCCM) of Cα atoms of residues 35–180 in simulation **1** (A) and 33–180 in simulation **2** (B). We identify seven correlations between structural elements (C1–7, marked in white) that are conserved in the two simulations. Other correlations (C8, C9–10) and anticorrelations (A1–5, A6–11) are found only in one simulation. Cartoon representations of the correlations are given in Figure S6.

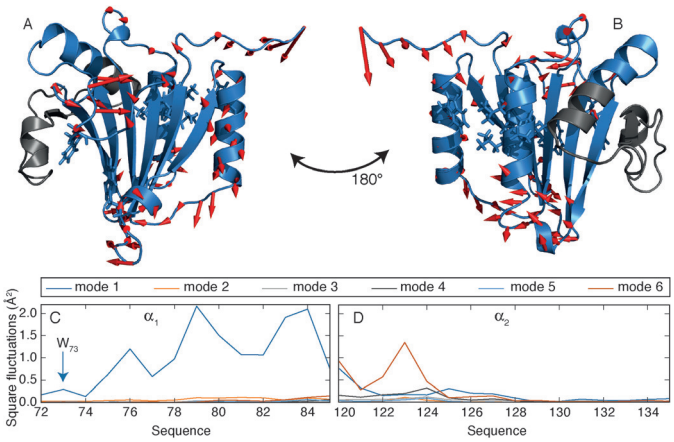

Figure 3. A, B) First PC in simulation **2**. The part of the protein not included in the analysis is colored in grey. C, D) Square fluctuations in α1 (C) and α2 (D) owing to the first six modes in simulation **2**.

The four modes of simulation **1** involve mostly the loops of the cap-binding site (Figure S8), residues between α1 and β3, including the 3/10 helix, and residues in the β4–α2 loop (Figure S10). α1 and α2 participate to a much smaller extent. The modes involve a similar set of residues as the A1–5 anticorrelations, but the role of helices and β-strands is much more evident in DCCMs, which are normalized by the fluctuation amplitude.

Similar to the NMR data in Figure 1, Figures S9 and S11 show that the fluctuations are spread across the sequence in simulation **2**. Interestingly, dynamic behavior is found for those residues with side chains that were shown to be affected by 4EGI-1 binding.[17] The N-terminal part of α3, as well as the β5–β6 loop, are involved in motions. Most of the residues contributing to the correlated dynamics in Figure 2, particularly C9-10 and A6-11, also contribute to the modes in Figure S11.

A close look at mode 1 (Figure 3 A,B) shows the role of α1. In fact, similar to A7, A9, and A10 above, the N terminus and the β1–β2 and β4–α2 loops are anticorrelated with the C-terminal end. The loop bearing W_{102} also contributes to this mode. Crucially, these motions are transferred to the binding site by correlations within α1 (C10). In fact, fluctuations in α1 are larger in simulation **2** (Figure 3 C) than simulation **1** (Figure S8), mostly at the C-terminal end, but significantly also for W_{73} and F_{72}. On the other hand, Figure 3 D confirms that motions in the flexible N-terminal end of α2 are hardly transferred to the binding site, which remains rigid.

The projection of simulations **1_25C** and **2_25C** onto the PC space (Figures S12 and S13) is very similar to that of simulations **1** and **2**, thus suggesting that the results of our analysis do not depend on temperature in physiologically-relevant ranges.

In conclusion, similar to other proteins,[22] structure-encoded dynamics underlie the binding of eIF4E to its partners. 4EGI-1 triggers structural rearrangements that increase the flexibility in α1, coupling its fluctuations to the cap and 4EGI-1 binding sites and the N terminus. This modulates the distance between the two parts of the eIF4G binding site on α1 and α2, which might result in the inhibitory effect, without affecting the structure of the eIF4G binding site.

This new model for the activity of 4EGI-1, which was developed by using NMR relaxation data and MD simulations and is compatible with experimental evidence accumulated over the years,[13,14,17,21,23] might inspire alternative routes to inhibition of the eIF4E/eIF4G interaction. While our work is focused on backbone dynamics, experimental and computational studies on side chains might be a powerful way of elucidating the details of the mechanism. The pervasive role of the β3–β4 loop in all collective motions might indicate a potential effect of 4EGI-1 on binding to the cap, a hypothesis that deserves further investigation.

Acknowledgements

N.S. acknowledges a European Molecular Biology Organization Long-Term Fellowship (ALTF 612-2013) and a Swiss National Science Foundation Early Postdoc.Mobility Fellow-

ship (P2ELP2_148858). This research was supported by National Institutes of Health Grants PO1 GM047467, P41-EB002026, and RO1 CA68262, CEA (Commissariat à l'Energie Atomique et aux Energies Alternatives) and CNRS (Centre National de la Recherche Scientifique). M.D. simulations were performed using the HPC resources of CCRT available by GENCI (Grand Equipement National de Calcul Intensif, project t2015077486).

Keywords: allosterism · inhibitors · molecular dynamics · NMR spectroscopy · protein–protein interactions

How to cite: *Angew. Chem. Int. Ed.* **2016**, *55*, 7176–7179
Angew. Chem. **2016**, *128*, 7292–7295

[1] D. Silvera, S. C. Formenti, R. J. Schneider, *Nat. Rev. Cancer* **2010**, *10*, 254–266.
[2] M. Bhat, N. Robichaud, L. Hulea, N. Sonenberg, J. Pelletier, I. Topisirovic, *Nat. Rev. Drug Discovery* **2015**, *14*, 261–278.
[3] J. Marcotrigiano, A. C. Gingras, N. Sonenberg, S. K. Burley, *Mol. Cell* **1999**, *3*, 707–716.
[4] Y. Martineau, R. Azar, C. Bousquet, S. Pyronnet, *Oncogene* **2013**, *32*, 671–677.
[5] E. Petroulakis, A. Parsyan, R. J. O. Dowling, O. LeBacquer, Y. Martineau, M. Bidinosti, O. Larsson, T. Alain, L. Rong, Y. Mamane, et al., *Cancer Cell* **2009**, *16*, 439–446.
[6] R. J. O. Dowling, I. Topisirovic, T. Alain, M. Bidinosti, B. D. Fonseca, E. Petroulakis, X. Wang, O. Larsson, A. Selvaraj, Y. Liu, et al., *Science* **2010**, *328*, 1172–1176.
[7] B. C. Barnhart, M. C. Simon, *J. Clin. Invest.* **2007**, *117*, 2385–2388.
[8] C. A. Dumstorf, B. W. Konicek, A. M. McNulty, S. H. Parsons, L. Furic, N. Sonenberg, J. R. Graff, *Mol. Cancer Ther.* **2010**, *9*, 3158–3163.
[9] S. B. Korets, S. Czok, S. V. Blank, J. P. Curtin, R. J. Schneider, *Clin. Cancer Res.* **2011**, *17*, 7518–7528.
[10] L. Furic, L. Rong, O. Larsson, I. H. Koumakpayi, K. Yoshida, A. Brueschke, E. Petroulakis, N. Robichaud, M. Pollak, L. A. Gaboury, et al., *Proc. Natl. Acad. Sci. USA* **2010**, *107*, 14134–14139.
[11] G. Armengol, F. Rojo, J. Castellví, C. Iglesias, M. Cuatrecasas, B. Pons, J. Baselga, S. Ramón y Cajal, *Cancer Res.* **2007**, *67*, 7551–7555.
[12] J. R. Graff, B. W. Konicek, R. L. Lynch, C. A. Dumstorf, M. S. Dowless, A. M. McNulty, S. H. Parsons, L. H. Brail, B. M. Colligan, J. W. Koop, et al., *Cancer Res.* **2009**, *69*, 3866–3873.
[13] N. J. Moerke, H. Aktas, H. Chen, S. Cantel, M. Y. Reibarkh, A. Fahmy, J. D. Gross, A. Degterev, J. Yuan, M. Chorev, et al., *Cell* **2007**, *128*, 257–267.
[14] N. Sekiyama, H. Arthanari, E. Papadopoulos, R. A. Rodriguez-Mias, G. Wagner, M. Léger-Abraham, *Proc. Natl. Acad. Sci. USA* **2015**, *112*, E4036–45.
[15] T. Yi, E. Kabha, E. Papadopoulos, G. Wagner, *Oncotarget* **2014**, *5*, 6028–6037.
[16] L. Chen, B. H. Aktas, Y. Wang, X. He, R. Sahoo, N. Zhang, S. Denoyelle, E. Kabha, H. Yang, R. Y. Freedman, et al., *Oncotarget* **2012**, *3*, 869–881.
[17] E. Papadopoulos, S. Jenni, E. Kabha, K. J. Takrouri, T. Yi, N. Salvi, R. E. Luna, E. Gavathiotis, P. Mahalingam, H. Arthanari, et al., *Proc. Natl. Acad. Sci. USA* **2014**, *111*, E3187–95.
[18] J. A. McCammon, S. C. Harvey, *Dynamics of Proteins and Nucleic Acids*, Cambridge University Press, Cambridge, **1988**.
[19] O. F. Lange, H. Grubmüller, *Proteins Struct. Funct. Bioinf.* **2006**, *62*, 1053–1061.
[20] G. Bouvignies, P. Bernado, S. Meier, K. Cho, S. Grzesiek, R. Bruschweiler, M. Blackledge, *Proc. Natl. Acad. Sci. USA* **2005**, *102*, 13885–13890.
[21] N. Siddiqui, W. Tempel, L. Nedyalkova, L. Volpon, A. K. Wernimont, M. J. Osborne, H.-W. Park, K. L. B. Borden, *J. Mol. Biol.* **2012**, *415*, 781–792.
[22] K. Henzler-Wildman, D. Kern, *Nature* **2007**, *450*, 964–972.
[23] D. Peter, C. Igreja, R. Weber, L. Wohlbold, C. Weiler, L. Ebertsch, O. Weichenrieder, E. Izaurralde, *Mol. Cell* **2015**, *57*, 1074–1087.

Received: April 3, 2016
Published online: May 10, 2016

